Journal of Materials Chemistry C

The layered RuBr3-RuI3 honeycomb system

Journal:	*Journal of Materials Chemistry C*
Manuscript ID	TC-ART-12-2023-004718.R1
Article Type:	Paper
Date Submitted by the Author:	09-Feb-2024
Complete List of Authors:	Ni, Danrui; Princeton University, Chemistry Xu, Xianghan; Princeton University, Chemistry Cava, Robert; Princeton University, Department of Chemistry

The layered $RuBr_3$-RuI_3 honeycomb system

Danrui Ni, Xianghan Xu, Robert J. Cava*

Department of Chemistry, Princeton University, Princeton, NJ 08544, USA

*E-mail: rcava@princeton.edu

Abstract

The layered $RuBr_3$-RuI_3 honeycomb structure solid solution was synthesized at high-pressures. The crystal structures are centrosymmetric (space group *R*-3) and based on honeycomb layers of spin ½ Ru^{3+}. The solid solution switches from insulating to metallic between $RuBr_{0.75}I_{2.25}$ and $RuBr_{0.50}I_{2.50}$. A preliminary structure/property phase diagram is presented. Our results suggest that this solid solution may provide insight into the influence of disorder on spin-orbit-coupled quantum spin liquids.

Keywords: ruthenium trihalide, honeycomb layer, solid solution, high pressure synthesis, magnetic frustration

1.Introduction

Spin systems based on triangular motifs have attracted much attention in recent decades, as qualitatively new states of matter can sometimes result[1–4]. Thus the honeycomb lattice with *S*=1/2 has recently been in the spotlight due to the prediction that there might be quantum spin liquid states in such lattices[5], which include a family of spin–orbit assisted Kitaev materials[6,7], with honeycomb-layer-structured α-$RuCl_3$ emerging as a potential candidate for displaying that kind of physics[8–10]. The magnetic frustration, as well as the disorder, whose role remains understudied and may introduce further complex interplay among different parameters, can lead to unconventional quantum critical phenomena and multiple phases[11,12]. Here, to further explore a honeycomb based magnetic frustrated system, and test the effects of metal-halide hybridization on the properties, we study the solid solution between $RuBr_3$ and RuI_3, which both crystallize in a 1D-chain structure at ambient pressure[13] and both of which transform into a honeycomb layered phase under moderately high pressure[14–17]. With similar layered structures, honeycomb-based $RuBr_3$ and RuI_3 are reported to exhibit distinct physical properties, as $RuBr_3$ is an insulator with an antiferromagnetic ordering transition while α-RuI_3 is a metal with weakly paramagnetic behavior and no magnetic ordering down to 1.8 K[15,16,18,19]. With Br being more similar in size to I than Cl is, we expect the $RuBr_3$-RuI_3 system to be more suitable for the formation of a solid solution than the analogous $RuCl_3$-RuI_3 honeycomb system. Thus, in order to probe the insulator to metal transition, here we present the crystal structures

and elementary properties of the honeycomb-layered α-Ru$(Br_{1-x}I_x)_3$ solid solution synthesized by a high pressure method. A honeycomb layered structure is found for each compound, and their physical properties reveal a strong variation with composition.

2.Experimental

Amorphous RuI_3 (Sigma-Aldrich, anhydrous, 99%) and crystalline $RuBr_3$ (Alfa Aesar, anhydrous, $\geq$ 98%) were used as starting materials. The powders were mixed well in stoichiometric ratios and loaded into boron nitride crucibles. The mixtures were then inserted into a pyrophillite cube assembly, pressed to 6 GPa using a cubic multi-anvil system (Rockland Research Corporation), and heated to 800 °C at 50 °C/min with temperature determined by an internal thermocouple. The samples were kept at 800 °C for 3 hours and then quench-cooled before decompression. The products obtained were black and relatively stable in air. Small single crystals could be isolated in the post-reaction samples and were used for the single crystal X-ray diffraction characterization, while as-made dense pieces were saved for the magnetization, resistivity and heat capacity measurements.

A vapor transport method was employed on some of the post-synthesis samples to rid them of a small amount of chemical impurity, presumably introduced due to its presence in the starting materials. For this process, the samples were sealed in a quartz tube under vacuum with the hot end at 250 °C and the cold end at ambient temperature. The impurity was transferred to the cold end, and the honeycomb-layer structured solid solution samples were maintained in the hot zone with no signs of decomposition or phase transformation.

Single-crystal X-ray diffraction (SCXRD) was performed at 295 K using a Bruker D8 Quest Eco diffractometer equipped with a Photon III CPAD detector and monochromated Mo Kα radiation (λ= 0.71073Å). The refinement was performed by using the SHELXTL Software Package[20,21]. Powder X-ray diffraction (PXRD) characterizations were carried out on a Bruker D8 Advance Eco with Cu Kα radiation (λ = 1.5406 Å), and the Le Bail fitting of the acquired PXRD patterns was conducted via the TOPAS software.

Magnetization and heat capacity data were collected using a Quantum Design (QD) Dynacool PPMS-9, equipped with a vibrating sample magnetometer (VSM) option. Resistivity was also measured on QD Dynacool PPMS, using a four-probe method, and electrodes were made by silver epoxy. The magnetic field applied for the temperature-dependent magnetization measurements was 1000 Oe, and the magnetic susceptibility was defined as M/H where M is the measured Magnetization and H is the applied magnetic field. For the AC susceptibility measurements, a varying field of 4 Oe amplitude was applied with a DC bias field of 10 Oe.

3.Results and Discussion

The layered α-Ru$(Br_{1-x}I_x)_3$ honeycomb solid solution was synthesized by the high-pressure high-temperature method. A *R*-3 honeycomb layer structure was found by SCXRD for all compositions (**Figure 1A**) There is no sign of a missing center of symmetry in our experiments,

and the bromine and iodine atoms appear to be totally disordered in all our mixed anion materials, occupying the same site in the unit cell. The crystallographic information and refined parameters of the solid solutions are listed in **Tables 1** and **S1-S2**. One structural detail is noted, which is that for most of the refined structures, the normally empty interstitial sites (Ru2, Wyckoff position 3*a*) in this three-layer unit cell are occupied on average by a small percentage of Ru atoms. This disordering of the Ru is most likely due to the presence of a small number of two-layer stacking faults in this three-layer structure, visible as a small number of Ru interstitials because diffraction experiments of the type performed here are a positional average over the whole crystal. The presence of stacking faults like these is commonly observed in similar van der Waals layered-structure systems [16,22] so we are not surprised to see them here. The amount of Ru on the 3*a* site, and thus the fraction of two-layer stacking faults, is below 5% for almost all of the materials in the solid solution, while it is slightly higher in $RuBr_{0.5}I_{2.5}$ (where about 87% of the Ru occupies the honeycomb lattice while 13% occupies the interstitial site), which may suggest that there is a higher degree of interlayer stacking errors in $RuBr_{0.5}I_{2.5}$. Without constraints among the occupancy parameters in the structure refinement, these honeycomb materials freely refine to be slightly Ru-deficient (ranging roughly from $Ru_{0.92}X_3$ to $Ru_{1.00}X_3$, where X = Br plus I). We conclude that more detailed structural study, designed to observe stacking faults or other structural errors in this solid solution, such as by high-resolution electron microscopy, may be of future interest.

The RuX_6 octahedron of the solid solution series is close to ideal symmetry with a very slight distortion. Based on the bond angle and bond length data in **Table S2**, the Ru-X distance increases with increasing I in the formula, as expected. Our PXRD characterization confirms the consistency of the bulk samples with the honeycomb structures observed by SCXRD, with the data for some representative compositions shown in **Figures 1B** and **S1.** The PXRD patterns indicate that they have the same structure type. In the materials with higher bromine content, a small amount of layered $RuBr_3$ phase shows up as an impurity in the PXRD pattern (**Figure S1**). Compared to the end-member compounds, longer annealing time (3 hours) is required for the solid solutions to obtain a relatively uniform phase. (With shorter annealing times (1 hour), lower diffraction intensity and wider diffraction peaks are observed in the products' PXRD patterns suggesting that a chemical composition distribution may be present if the samples are not heated long enough.)

The magnetic susceptibility (M/H) was measured on polycrystalline samples at temperatures between 1.8 and 300 K (**Figure 2A**). Although all display a small upturn of magnetization at low temperature, typically attributed to a very small number of uncorrelated "orphan" spins[23], the materials in the α-$Ru(Br,I)_3$ solid solution can straightforwardly be divided into Br-rich and I-rich groups based on their magnetic behavior. The Br-rich compositions, whose magnetism is more strongly temperature-dependent, have a stronger magnetic response and clearer anomalies than the I-rich samples (with magnetism essentially temperature-independent). Among the solid solution materials, the material with composition $RuBr_2I$ ($Ru(Br_{.67}I_{.33})_3$) gives the highest magnetic susceptibility at low temperatures (its susceptibility at 100 K. We note that the 2:1

ratio of X ions is particularly interesting to us as it has the potential for short range ordering in this three-fold symmetry system.

In the Br-rich group, the temperature of the susceptibility anomaly (T_A) is around 32 K for α-$RuBr_3$, and 25-27 K for the solid solutions. This temperature range is labeled with different colors in **Figure 2A** for comparison. The decrease in temperature of the susceptibility anomaly may be interpreted as saying that by introducing iodine with disordered occupancy into the system, the frustration and randomness increase and thus suppress the ordering transition. To confirm that the magnetization anomalies observed in the layered honeycomb solid solution are not present due to the presence of a small amount of the ambient pressure phase, an ambient pressure synthesis and magnetic characterization of 1D-chain structure "$RuBr_2I$" was also conducted (**Figure S2**), and no magnetic ordering down to 1.8 K was observed, indicating that the anomalies in **Figure 2A** can't arise from the presence of an adventitious 1D chain phase. In contrast, the I-rich group shows relatively weak paramagnetic behavior over a wide temperature range, especially for samples with $x \geq 0.75$, which have no 3D magnetic ordering features visible down to 1.8 K.

While the I-rich samples show non-Curie-Weiss behavior in their magnetism even up to 300 K, Curie-Weiss fitting to the magnetic susceptibility in the high temperature range (150 – 300 K) for the Br-rich samples was carried out to further explore their magnetism (**Figure 2B** and **Figure S3**) using the following equation:

$$\chi - \chi_0 = \frac{C}{T - \theta} \qquad (1)$$

Some of the important fit parameters are listed in **Table 2**. The effective moment per Ru (μ_{eff}), is larger than the theoretical value of a spin-only *S*=1/2 system (μ_s = 1.73), suggesting an obvious contribution of the orbital interaction, thus confirming the expected non-negligible spin orbit coupling in the system. Additionally, based on the fitting results, $RuBr_{1.5}I_{1.5}$, the composition with the largest degree of Br-I mixing disorder, gives the largest frustration parameter. We thus deduce that the disorder induced by the off-magnetic-site mixing of nonmagnetic Br and I may affect the magnetic ground state of this honeycomb-based material by introducing disorder in the bond lengths and angles, which would change the energy states and orbital overlap. Also, when varying from bromine to the same-column-of the periodic-table heavier element iodine, the changes in spin-orbit physics and the Ru-ligand interactions can lead to differences in the electronic structures of the compound. This may contribute to the different properties of Br-rich samples compared to those that are I-rich. This is analogous to the observation in a nickel oxyhalide system in 2022[24], where researchers demonstrated a long-range magnetically ordered state for anion-ordered Sr_2NiO_3Cl, and a short-range magnetically ordered state of anion-disordered Sr_2NiO_3F. The later compound was reported to exhibit spin-glass-like behavior with an anomaly at much lower temperature, and no long-range magnetic ordering was observed. With this in mind it may be of future interest to further explore the Ru-

X interactions and the origin of the electronic band structure variations for the disordered α-$Ru(Br,I)_3$ solid solution.

It is noted that the atypically large μ_{eff} and θ values that these Curie-Weiss fittings find may suggest that the spin coupling in the α-$Ru(Br,I)_3$ system doesn't perfectly follow the standard Curie-Weiss law[18], and the fitting results here can be taken as an approximation. Because for a magnetic honeycomb lattice, relatively large frustration parameters and the deviation of zero-field-cooled (ZFC) and field-cooled (FC) curves suggest that the solid solution system may adopt spin-glass-like behavior[25,26], AC susceptibility measurements were conducted on an α-$RuBr_2I$ sample. As presented in **Figure 2C**, these measurements show a variation with changing frequency, consistent with magnetic glassiness in the system. This is not surprising, as it is well established that disorder can lead to a spin-glass ground state. According to the theoretical literature, however, a frustrated system with both disorder and strong spin-orbit coupling can result in the emergence of different quantum-spin phenomena. Chemical disorder and the resulting randomization of magnetic interactions can enhance quantum fluctuations in a magnetic honeycomb system[27], suppress the long-range order, and lead to defect-induced frozen magnetic degrees of freedom[28]; inducing mimicry of a spin-liquid state in some materials[29]. The heat capacity data for honeycomb-layered α-$Ru(Br,I)_3$, collected between 2 and 150 K, presented in **Figure S4**, show no anomalies, suggesting the suppression of long-range order in this system. Further exploration of the spin-orbit physics of this disordered layered honeycomb solid solution system may therefore be of future research interest to experts in that area of study.

The M vs H curves for different members of the solid solution were measured at 2 K and 250 K and are plotted in **Figure 3** and **Figure S5**. Same as the magnetic susceptibility, the α-$Ru(Br,I)_3$ solid solution can be roughly divided into Br-rich and I-rich groups based on their behavior. Samples show linear magnetization response with changing magnetic field at 250 K, as expected. However, at 2 K, a weak S-shape at lower fields can be observed for I-rich formulas (**Figure 3B**, with individual views in **Figure S6**), while the Br-rich samples tend to show more linear response in M vs H, with a small hysteretic opening of the curve (**Figure 3C**). It is known that an S-shaped character will be displayed by materials where the available spins and the magnetization follow a Brillouin function relationship[30], which however is not the case for the α-$Ru(Br,I)_3$ solid solution. Our data therefore suggest that the $RuBr_3$-RuI_3 honeycomb solid solution seems to be far from an ideal paramagnetic system and that the Ru spins present in the materials cannot be considered as isolated[16].

Resistivity measurements were carried out to characterize the transport properties of the solid solution, and to determine the transition point from an insulator to a metal. In **Figure 4**, the normalized resistivity of the α-$Ru(Br_{1-x}I_x)_3$ series is plotted versus temperature from 125 to 275 K (to rule out the influence of surface moisture), and the inset shows the enlarged views of the iodine-rich group (The magnitude of resistivity at 275 K is presented in **Figure S7**). It is clear that the alloyed compounds show insulating behavior at the higher Br contents, as their resistivities

decrease with increasing temperature. But for x = 0.83 ($RuBr_{0.5}I_{2.5}$), the compound behaves as a bad metal (resistivities increase with increasing temperature, but with a different trend compared to typical metallic materials). Generally, the resistivity decreases with increasing iodine ratio (except for the x = 0.5, $RuBr_{1.5}I_{1.5}$ sample), which is consistent with the transition from an insulator to metal; the crossover from insulating to metallic behavior is located between x = 0.75 and x = 0.83. For insulating formulas, the resistivity activation energy values are calculated based on the linear fitting of high temperature range selected from ln(ρ) vs 1/T plots, and are listed in **Table 2**. The decrease of the activation energy value with increasing iodine content supports a gradual insulator-to-metal transition in the system; a more obvious metallic component is seen for the iodine-rich group, especially for x ≥ 0.75, as the nonlinear shape of the ln(ρ) vs 1/T curve may suggest an unneglectable metallic contribution (**Figure S8**).

Summarizing the structural and physical properties or the honeycomb-layered α-$Ru(Br_{1-x}I_x)_3$ solid solution, a phase diagram can be drawn (**Figure 5**.) Both *a* and *c* of the *R*-3 unit cell initially show relatively linear increase with increasing x but are then nonlinear when x is higher than 0.67, resulting a maximum of *c*/*a* at around x = 0.25 (*c*/*a*, a measure of the structural dimensionality, is frequently used to characterize layered materials); the solid solution system is more complicated than predicted by simple size-mixing expectations. No matter what the details are, the phase diagram reveals an evolution of the solid solution from a more $RuBr_3$-like behavior into a more RuI_3-like type behavior, and, when x > 0.67, from that of a stronger magnetic response with short-range correlations (localized magnetism with Curie-Weiss-type behavior in the high temperature range measured), to a weakly paramagnetic behavior with no clear magnetic ordering (more and more delocalized and itinerant magnetism, with behavior not following the Curie-Weiss Law at high temperature) labeled as the orange-colored area, and changing from an insulator to a metal at the relatively high Iodine content of x = 0.83 (the shaded area).

4. Conclusion

The layered honeycomb α-$Ru(Br_{1-x}I_x)_3$ solid solution with varying x was prepared by high pressure synthesis. Their *R*-3 unit cells were characterized by SCXRD, and their magnetic and transport properties were determined. The variation with changing I to Br ratio was thus revealed, including an insulator-to-metal transition between $RuBr_{0.75}I_{2.25}$ and $RuBr_{0.5}I_{2.5}$, accompanied by a dramatic change in the magnetic properties. By introducing the disorder of halogen atoms, the frustration and randomness increased, triggering short-range magnetic correlations and what may be spin-glass-like behavior. This solid solution system may provide insight into the spin/orbit interaction in a spin ½ Ru-based system with disordered halogens. It may be of future interest to perform NMR studies on these materials. Further, more generally, this system may provide a new venue for studying quantum spin phenomena with disorder and strong spin-orbit coupling for both magnetic frustrated insulators and metals, and thus may open a door to further understanding and modifying the interaction of spin and orbital degrees of freedom of honeycomb-based systems. As it remains an open question how the ground

states of the highly correlated, strongly fluctuating magnetic phases are affected by disorder, future more detailed study may be of interest. Our results suggest that isovalent anion doping can trigger a complicated interplay among the electronic and magnetic states in quantum materials.

Note added: During the review of this manuscript we noted related work[31] on this system..

Acknowledgement

This research was funded by the Gordon and Betty Moore Foundation, EPiQS initiative, Grant No. GBMF-9066. X. Xu acknowledges the US Department of Energy grant DE-FG-02-98ER45706.

Appendix

CCDC numbers 2299103-2299108 contain the crystallographic data, which can be obtained free of charge (available at www.ccdc.cam.ac.uk/data_request/cif, or by emailing data_request@ccdc.cam.ac.uk, or by contacting The Cambridge Crystallographic Data Centre, 12 Union Road, Cambridge CB2 1EZ, UK, fax: + 441223336033).

Author Contributions

Danrui Ni: Conceptualization, Methodology, Investigation, Formal analysis, Visualization, Writing - Original Draft; **Xianghan Xu:** Validation, Methodology, Investigation, Formal analysis, Software, Writing - Reviewing and Editing; **Robert J. Cava*:** Conceptualization, Methodology, Data curation, Resource, Supervision, Project administration, Funding acquisition, Writing-Reviewing and Editing.

Conflicts of interest

The authors declare that they have no known competing financial interests or personal relationships that could have appeared to influence the work reported in this paper.

References

1 J. Snyder, J. S. Slusky, R. J. Cava and P. Schiffer, *Nature*, 2001, **413**, 48–51.
2 S.-H. Lee, C. Broholm, W. Ratcliff, G. Gasparovic, Q. Huang, T. H. Kim and S.-W. Cheong, *Nature*, 2002, **418**, 856–858.
3 L. Balents, *Nature*, 2010, **464**, 199–208.
4 D. Billington, D. Ernsting, T. E. Millichamp, C. Lester, S. B. Dugdale, D. Kersh, J. A. Duffy, S. R. Giblin, J. W. Taylor, P. Manuel, D. D. Khalyavin and H. Takatsu, *Sci Rep*, 2015, **5**, 12428.
5 A. Kitaev, *Annals of Physics*, 2006, **321**, 2–111.
6 K. Kitagawa, T. Takayama, Y. Matsumoto, A. Kato, R. Takano, Y. Kishimoto, S. Bette, R. Dinnebier, G. Jackeli and H. Takagi, *Nature*, 2018, **554**, 341–345.
7 S. Trebst and C. Hickey, *Physics Reports*, 2022, **950**, 1–37.

8 H.-S. Kim, V. S. V., A. Catuneanu and H.-Y. Kee, *Phys. Rev. B*, 2015, **91**, 241110.
9 S.-H. Baek, S.-H. Do, K.-Y. Choi, Y. S. Kwon, A. U. B. Wolter, S. Nishimoto, J. van den Brink and B. Büchner, *Phys. Rev. Lett.*, 2017, **119**, 037201.
10 A. Banerjee, J. Yan, J. Knolle, C. A. Bridges, M. B. Stone, M. D. Lumsden, D. G. Mandrus, D. A. Tennant, R. Moessner and S. E. Nagler, *Science*, 2017, **356**, 1055–1059.
11 M. Vojta, *Rep. Prog. Phys.*, 2018, **81**, 064501.
12 I. Kimchi, A. Nahum and T. Senthil, *Phys. Rev. X*, 2018, **8**, 031028.
13 H. G. von Schnering, K. Brodersen, F. Moers, H. K. Breitbach and G. Thiele, *Journal of the Less Common Metals*, 1966, **11**, 288–289.
14 F. Ersan, E. Vatansever, S. Sarikurt, Y. Yüksel, Y. Kadioglu, H. D. Ozaydin, O. Ü. Aktürk, Ü. Akıncı and E. Aktürk, *Journal of Magnetism and Magnetic Materials*, 2019, **476**, 111–119.
15 Y. Imai, K. Nawa, Y. Shimizu, W. Yamada, H. Fujihara, T. Aoyama, R. Takahashi, D. Okuyama, T. Ohashi, M. Hagihala, S. Torii, D. Morikawa, M. Terauchi, T. Kawamata, M. Kato, H. Gotou, M. Itoh, T. J. Sato and K. Ohgushi, *Phys. Rev. B*, 2022, **105**, L041112.
16 D. Ni, X. Gui, K. M. Powderly and R. J. Cava, *Advanced Materials*, 2022, **34**, 2106831.
17 K. Nawa, Y. Imai, Y. Yamaji, H. Fujihara, W. Yamada, R. Takahashi, T. Hiraoka, M. Hagihala, S. Torii, T. Aoyama, T. Ohashi, Y. Shimizu, H. Gotou, M. Itoh, K. Ohgushi and T. J. Sato, *J. Phys. Soc. Jpn.*, 2021, **90**, 123703.
18 D. A. S. Kaib, K. Riedl, A. Razpopov, Y. Li, S. Backes, I. I. Mazin and R. Valentí, *npj Quantum Mater.*, 2022, **7**, 1–9.
19 Y. Choi, J.-H. Lee, S. Lee, D. Wulferding, H. Fujihara, F. Sato, Y. Imai, K. Ohgushi, M.-J. Seong and K.-Y. Choi, *Phys. Rev. B*, 2022, **106**, 174430.
20 G. M. Sheldrick, *Acta Crystallographica Section C Structural Chemistry*, 2015, **71**, 3–8.
21 G. M. Sheldrick, *Acta Cryst A*, 2015, **71**, 3–8.
22 T. Kong, K. Stolze, E. I. Timmons, J. Tao, D. Ni, S. Guo, Z. Yang, R. Prozorov and R. J. Cava, *Advanced Materials*, 2019, **31**, 1808074.
23 P. Schiffer and I. Daruka, *Phys. Rev. B*, 1997, **56**, 13712–13715.
24 Y. Tsujimoto, J. Sugiyama, M. Ochi, K. Kuroki, P. Manuel, D. D. Khalyavin, I. Umegaki, M. Månsson, D. Andreica, S. Hara, T. Sakurai, S. Okubo, H. Ohta, A. T. Boothroyd and K. Yamaura, *Phys. Rev. Mater.*, 2022, **6**, 114404.
25 K. Binder and A. P. Young, *Rev. Mod. Phys.*, 1986, **58**, 801–976.
26 J. W. Krizan and R. J. Cava, *Phys. Rev. B*, 2015, **92**, 014406.
27 R. Zhong, M. Chung, T. Kong, L. T. Nguyen, S. Lei and R. J. Cava, *Phys. Rev. B*, 2018, **98**, 220407.
28 R. Sibille, E. Lhotel, M. Ciomaga Hatnean, G. J. Nilsen, G. Ehlers, A. Cervellino, E. Ressouche, M. Frontzek, O. Zaharko, V. Pomjakushin, U. Stuhr, H. C. Walker, D. T. Adroja, H. Luetkens, C. Baines, A. Amato, G. Balakrishnan, T. Fennell and M. Kenzelmann, *Nat Commun*, 2017, **8**, 892.
29 Z. Zhu, P. A. Maksimov, S. R. White and A. L. Chernyshev, *Phys. Rev. Lett.*, 2017, **119**, 157201.
30 M. I. Darby, *Br. J. Appl. Phys.*, 1967, **18**, 1415.
31 F. Sato, H. Fujihara, H. Gotou, T. Aoyama, Y. Imai and K. Ohgushi, *Phys. Rev. B*, 2024, **109**, 035154.

Table 1. Atomic coordinates and equivalent isotropic displacement parameters for α-$Ru(Br,I)_3$ at 300 K. (U_{eq} is defined as one-third of the trace of the orthogonalized U_{ij} tensor (Å^2)). The standard deviations are indicated by the values in parentheses.

$Ru_{0.924}Br_{0.5}I_{2.5}$:

Atom	Wyck.	Occ.	*x*	*y*	*Z*	U_{eq}
I1	18*f*	0.8333	0.33449 (9)	0.32221 (10)	0.58703 (3)	0.0245 (3)
Br1	18*f*	0.1667	0.33449 (9)	0.32221 (10)	0.58703 (3)	0.0245 (3)
Ru1	6*c*	0.805 (6)	0.66667	0.33333	0.66677 (7)	0.0177 (6)
Ru2	3*a*	0.238 (9)	0.33333	0.66667	0.66667	0.028 (3)

$Ru_{1.009}Br_{0.75}I_{2.25}$:

Atom	Wyck.	Occ.	*x*	*y*	*z*	U_{eq}
I1	18*f*	0.75	0.66524 (11)	0.68219 (16)	0.41270(4)	0.0246 (8)
Br1	18*f*	0.25	0.66524 (11)	0.68219 (16)	0.41270(4)	0.0246 (8)
Ru1	6*c*	0.9771	0.33333	0.66667	0.33304 (8)	0.0242 (9)
Ru2	3*a*	0.063 (17)	0.66667	0.33333	0.33333	0.07 (3)

$Ru_{0.923}BrI_2$:

Atom	Wyck.	Occ.	*x*	*y*	*z*	U_{eq}
I1	18*f*	0.6667	0.6652 (2)	0.6822 (2)	0.41264 (6)	0.0255 (5)
Br1	18*f*	0.3333	0.6652 (2)	0.6822 (2)	0.41264 (6)	0.0255 (5)
Ru1	6*c*	0.906 (12)	0.33333	0.66667	0.33311 (14)	0.0201 (10)
Ru2	3*a*	0.033 (14)	0.66667	0.33333	0.33333	0.00 (3)

$Ru_{0.937}Br_{1.5}I_{1.5}$:

Atom	Wyck.	Occ.	*x*	*y*	*z*	U_{eq}
I1	18*f*	0.5	0.33458 (9)	0.31968 (10)	0.58770 (3)	0.0283 (3)
Br1	18*f*	0.5	0.33458 (9)	0.31968 (10)	0.58770 (3)	0.0283 (3)
Ru1	6*c*	0.896 (6)	0.66667	0.33333	0.66686 (6)	0.0203 (5)
Ru2	3*a*	0.081 (7)	0.33333	0.66667	0.66667	0.009 (6)

$Ru_{0.957}Br_2I$:

Atom	Wyck.	Occ.	*x*	*y*	*z*	U_{eq}

I1	18*f*	0.3333	0.68110 (12)	0.66541 (10)	0.58778 (4)	0.0267 (3)
Br1	18*f*	0.6667	0.68110 (12)	0.66541 (10)	0.58778 (4)	0.0267 (3)
Ru1	6*c*	0.951 (6)	0.66667	0.33333	0.66698 (6)	0.0196 (5)
Ru2	3*a*	0.012 (3)	0.33333	0.66667	0.66667	0.001

$Ru_{0.960}Br_{2.25}I_{0.75}$:

Atom	**Wyck.**	**Occ.**	***x***	***y***	***z***	U_{eq}
I1	18*f*	0.25	0.6654 (5)	0.6817 (6)	0.41209 (16)	0.0419 (10)
Br1	18*f*	0.75	0.6654 (5)	0.6817 (6)	0.41209 (16)	0.0419 (10)
Ru1	6*c*	0.960 (17)	0.33333	0.66667	0.3335 (4)	0.0344 (17)

Table 2. The magnetic anomaly temperature (T_A), Curie-Weiss temperature (θ), frustration parameter (f = |θ| / T_A), and the resistivity activation energy (E_a) calculated from linear fitting of the ln(ρ) vs 1/T curves, for α-$Ru(Br_{1-x}I_x)_3$. The activation energy value for x = 0 was obtained from Ref.11.

Iodine Fraction x	**T_A (K)**	**θ (K)**	***f***	**E_a (eV)**
0	32.3	-145	4.5	0.21[15]
0.25	27.1	-157	5.8	0.066
0.33	25.8	-322	12.5	0.054
0.5	25.6	-564	22.0	0.049
0.67	-	-	-	0.007
0.75	-	-	-	0.004

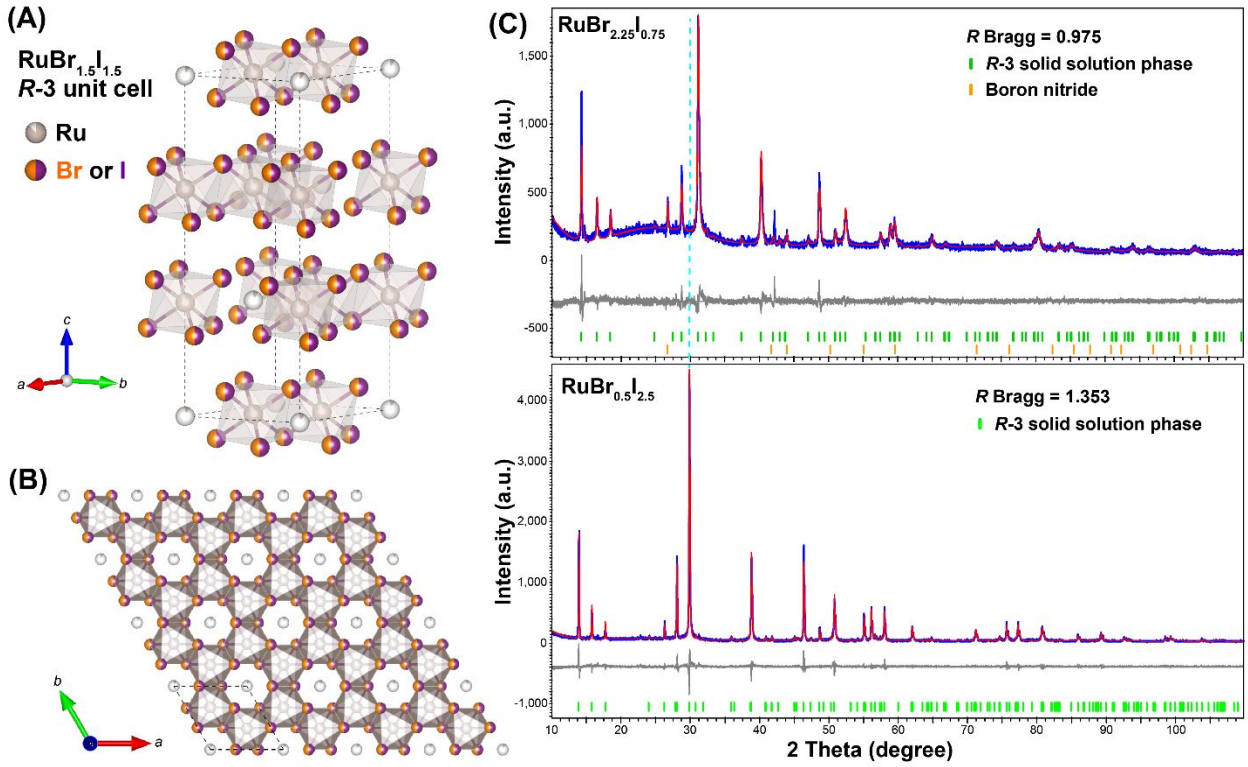

Figure 1. (A) The crystal structure of the honeycomb-layered α-$RuBr_3$-RuI_3 solid solution with a representative formula (x = 0.5 in $Ru(Br_{1-x}I_x)_3$) drawn, together with the view along the *c*-axis in **(B)**. **(C)** PXRD patterns with Le Bail fit for representative bulk $Ru(Br_{1-x}I_x)_3$ materials, confirming the consistency of the bulk sample structure and composition with the SCXRD refinement result. The dashed line shows the shift of the main peak position between the two patterns.

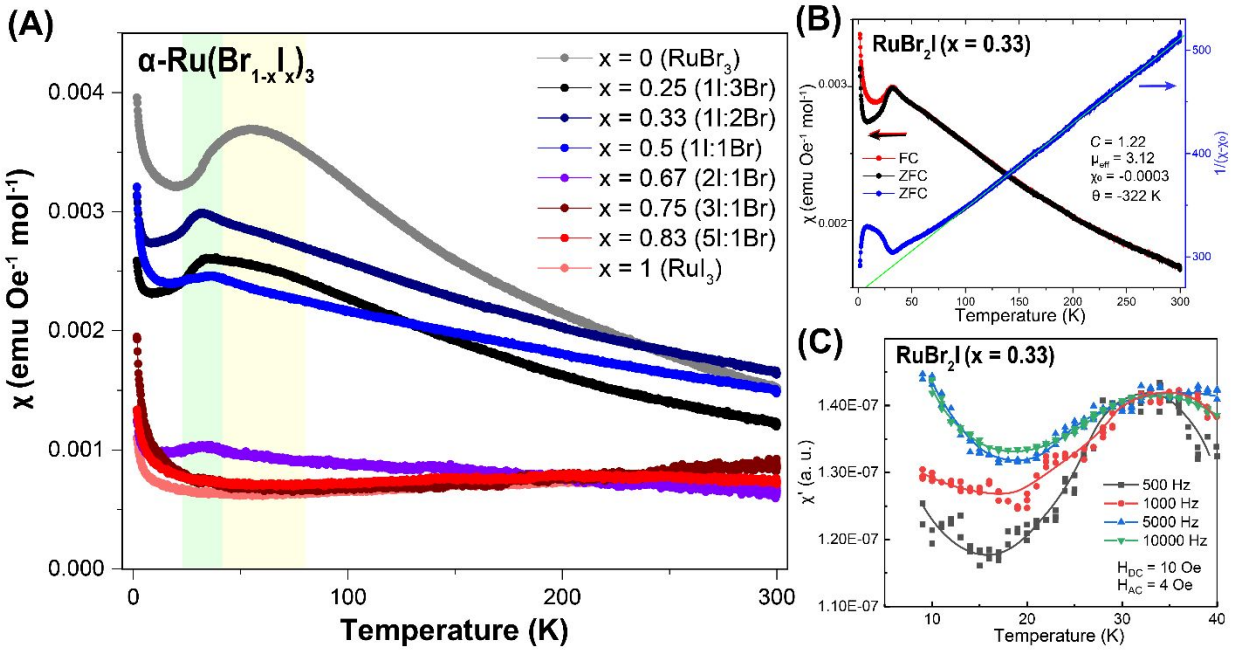

Figure 2. (A) The magnetic susceptibility measured from 1.8 to 300 K for the honeycomb-structure α-$Ru(Br_{1-x}I_x)_3$ solid solution series ($0 \le x \le 1$). Green colored shading marks the anomalies in the solid solution materials, while the yellow shading marks the anomaly in undoped α-$RuBr_3$. **(B)** Representative plot of the temperature dependent magnetic susceptibility χ (x = 0.33, ZFC in black and FC in red), together with the inverse of the difference between χ and the temperature-independent χ_0 in blue. Curie-Weiss fitting was conducted and the resulting parameters are shown in the panel. **(C)** The AC magnetic susceptibility data (χ′) collected on α-$RuBr_2I$ (x = 0.33) from 10 to 40 K, at various frequencies under a small DC field (10 Oe) with an AC field (4 Oe) applied.

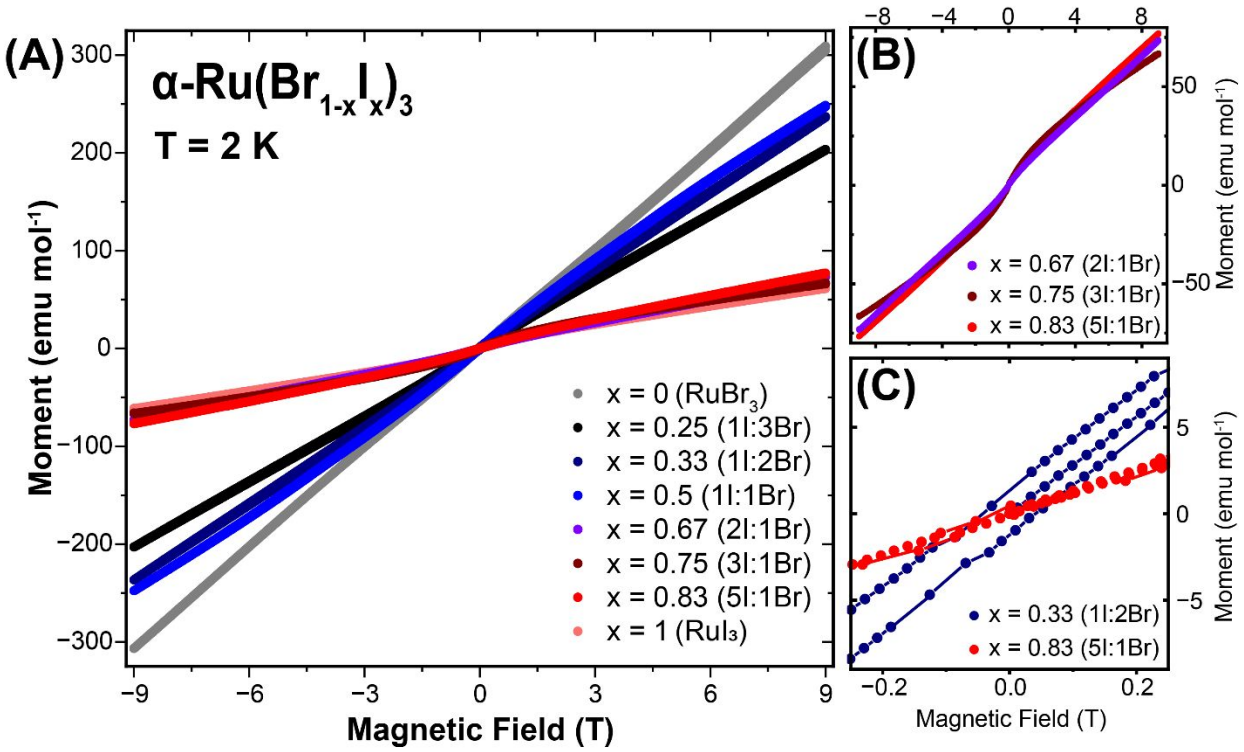

Figure 3. (A) The field-dependent magnetization data collected at 2 K for honeycomb-structure α-$Ru(Br_{1-x}I_x)_3$ ($0 \le x \le 1$), with the zoomed-in views of **(B)** the iodine-rich samples x = 0.67 to 0.83 to show the weak S-shape, and **(C)** x = 0.33 (Br-rich) and x = 0.83 (I-rich), revealing the very small hysteresis in this system.

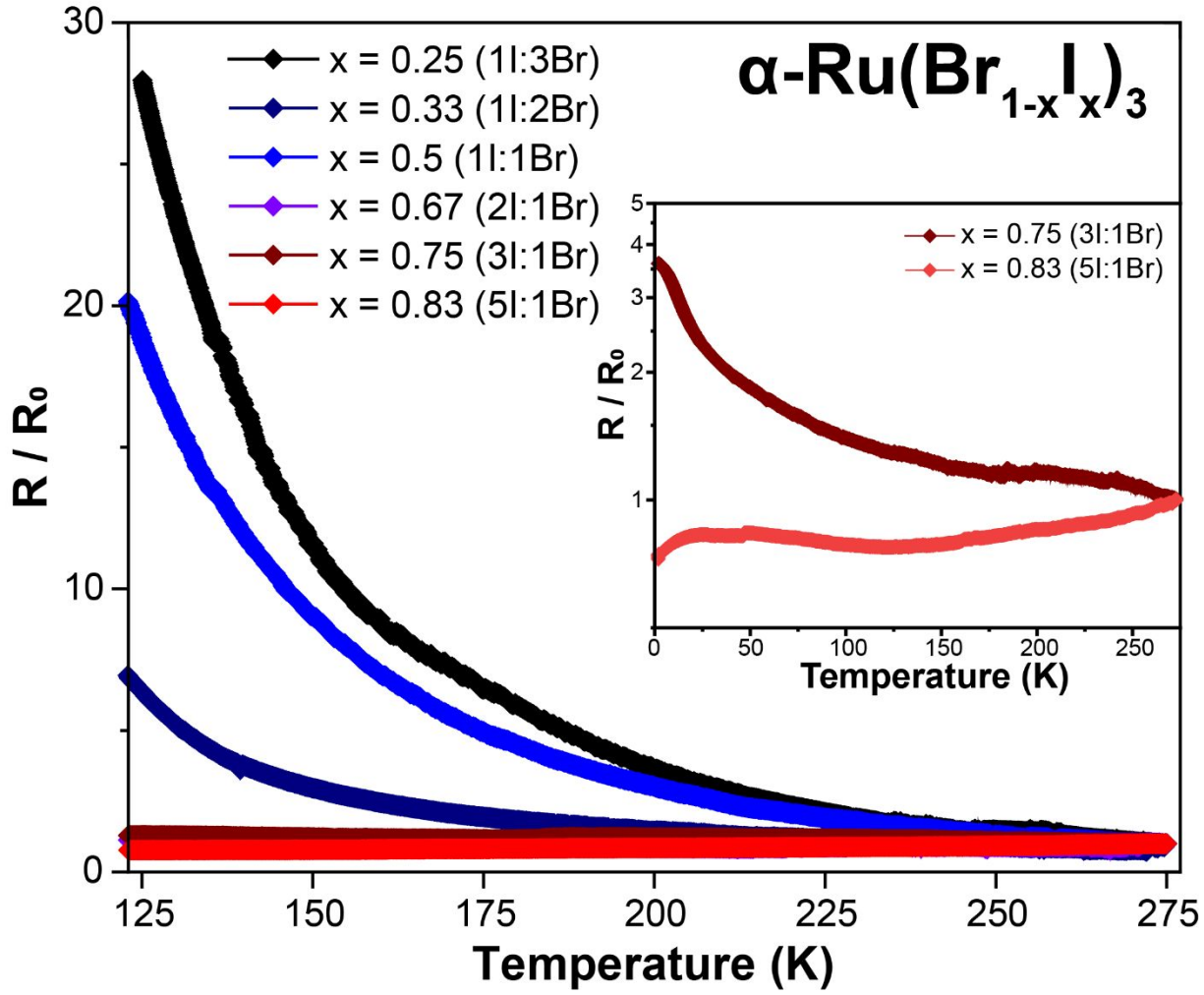

Figure 4. The normalized resistivity of the α-Ru($Br_{1-x}I_x$)$_3$ series plotted versus temperature from 125 to 275 K, with the inset showing the enlarged views in the 1.8 to 275 K range for the iodine-rich group near the insulator-to-metal switching point (x = 0.75 and x = 0.83). The magnitude of resistivity at 275 K of the solid solution is presented in Figure S7.

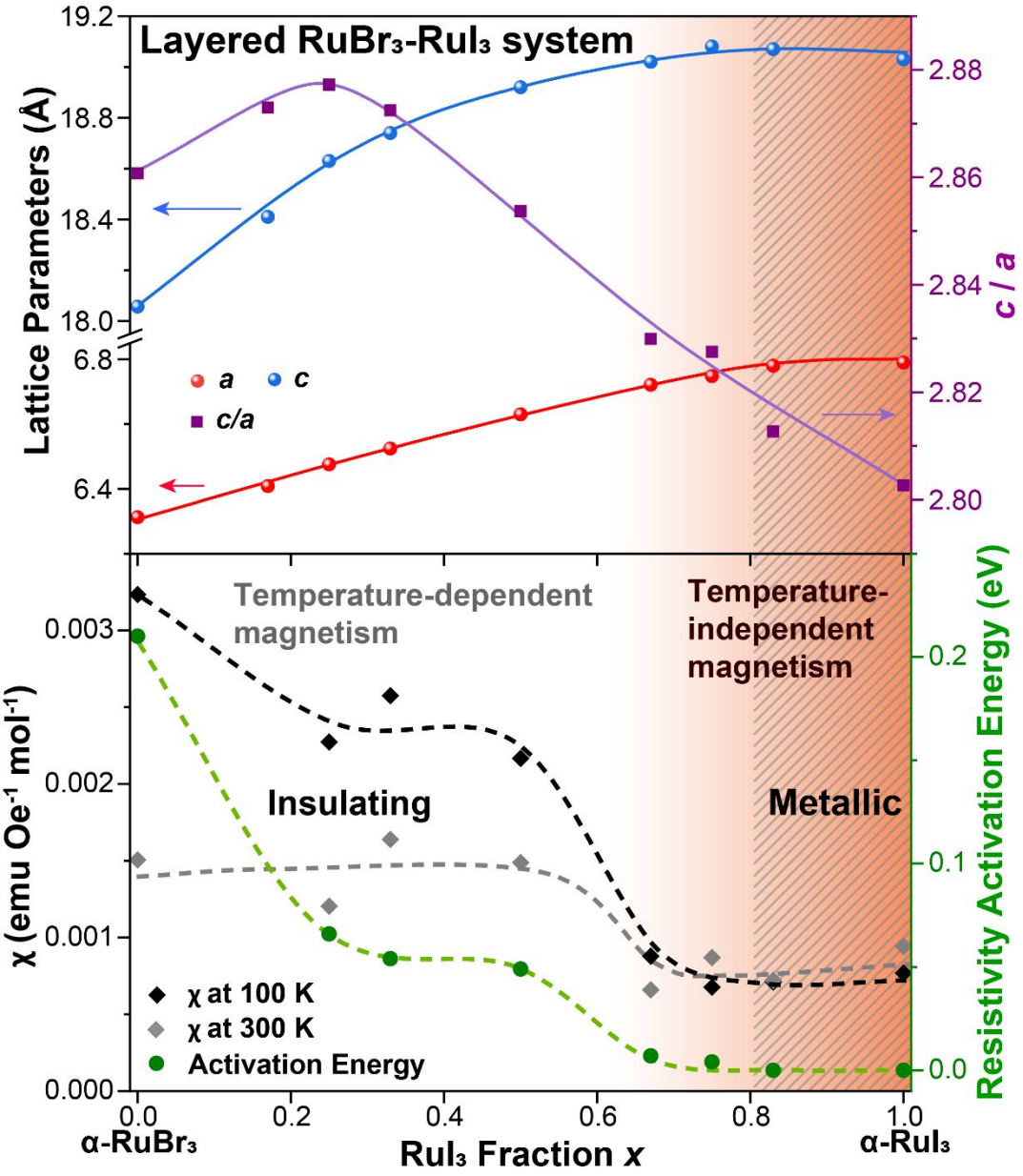

Figure 5. The tentative phase diagram for honeycomb-structure α-Ru($Br_{1-x}I_x$)$_3$ ($0 \le x \le 1$). Lattice parameters *a* and *c* are plotted versus x, together with *c*/*a*, in the upper part; magnetic susceptibility χ at 100 K and 300 K, and the resistivity activation energy (Table 1) are plotted in the lower part. From the white to orange-colored areas the solid solution material changes from localized temperature-dependent magnetic into being weakly paramagnetic with no clear magnetic transition; from the white to the shaded area it also changes from insulating to metallic.